

















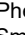
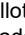






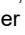
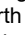











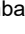




RESEARCH ARTICLE | NOVEMBER 14 2023

## Measurements of improved stability to achieve higher fuel compression in ICF

A. Do ; D. T. Casey ; D. S. Clark ; B. Bachmann ; K. L. Baker ; T. Braun ; T. M. Briggs; T. D. Chapman ; P. M. Celliers ; H. Chen ; C. Choate; E. L. Dewald ; L. Divol ; G. Fathi; D. N. Fittinghoff ; G. N. Hall ; E. Hartouni ; D. M. Holunga ; S. F. Khan ; A. L. Kritcher ; O. L. Landen ; A. G. MacPhee ; M. Millot ; E. V. Marley; J. L. Milovich ; A. Nikroo ; A. E. Pak; D. J. Schlossberg ; V. A. Smalyuk; M. Stadermann ; D. J. Strozzi ; R. Tommasini ; C. R. Weber ; B. N. Woodworth ; D. K. Yanagisawa; N. W. Birge ; C. R. Danly ; M. Durocher ; M. S. Freeman ; H. Geppert-Kleinrath ; V. Geppert-Kleinrath ; Y. Kim ; K. D. Meaney ; C. H. Wilde ; M. Gatu Johnson ; A. Allen ; M. Ratledge; C. Kong ; T. Fehrenbach ; C. Wild 



*Phys. Plasmas* 30, 112703 (2023)

<https://doi.org/10.1063/5.0167424>

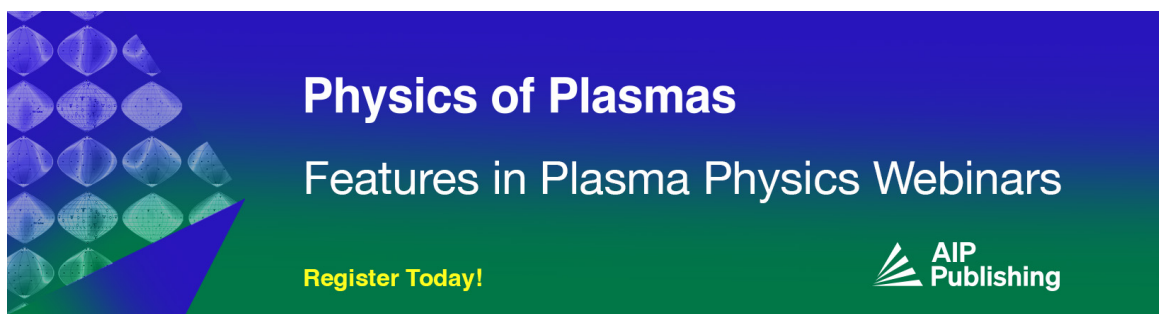


View  
Online




Export  
Citation

CrossMark



**Physics of Plasmas**  
Features in Plasma Physics Webinars

Register Today!



# Measurements of improved stability to achieve higher fuel compression in ICF

Cite as: Phys. Plasmas **30**, 112703 (2023); doi: 10.1063/5.0167424

Submitted: 12 July 2023 · Accepted: 20 October 2023 ·

Published Online: 14 November 2023



View Online



Export Citation



CrossMark

A. Do,<sup>1,a),b)</sup> D. T. Casey,<sup>1</sup> D. S. Clark,<sup>1</sup> B. Bachmann,<sup>1</sup> K. L. Baker,<sup>1</sup> T. Braun,<sup>1</sup> T. M. Briggs,<sup>1</sup> T. D. Chapman,<sup>1</sup> P. M. Celliers,<sup>1</sup> H. Chen,<sup>1</sup> C. Choate,<sup>1</sup> E. L. Dewald,<sup>1</sup> L. Divol,<sup>1</sup> G. Fathi,<sup>1</sup> D. N. Fittinghoff,<sup>1</sup> G. N. Hall,<sup>1</sup> E. Hartouni,<sup>1</sup> D. M. Holunga,<sup>1</sup> S. F. Khan,<sup>1</sup> A. L. Kritcher,<sup>1</sup> O. L. Landen,<sup>1</sup> A. C. MacPhee,<sup>1</sup> M. Millot,<sup>1</sup> E. V. Marley,<sup>1</sup> J. L. Milovich,<sup>1</sup> A. Nikroo,<sup>1</sup> A. E. Pak,<sup>1</sup> D. J. Schlossberg,<sup>1</sup> V. A. Smalyuk,<sup>1</sup> M. Stadermann,<sup>1</sup> D. J. Strozzi,<sup>1</sup> R. Tommasini,<sup>1</sup> C. R. Weber,<sup>1</sup> B. N. Woodworth,<sup>1</sup> D. K. Yanagisawa,<sup>1</sup> N. W. Birge,<sup>2</sup> C. R. Danly,<sup>2</sup> M. Durocher,<sup>2</sup> M. S. Freeman,<sup>2</sup> H. Geppert-Kleinrath,<sup>2</sup> V. Geppert-Kleinrath,<sup>2</sup> Y. Kim,<sup>2</sup> K. D. Meaney,<sup>2</sup> C. H. Wilde,<sup>2</sup> M. Gatju Johnson,<sup>3</sup> A. Allen,<sup>4</sup> M. Ratledge,<sup>4</sup> C. Kong,<sup>4</sup> T. Fehrenbach,<sup>5</sup> and C. Wild<sup>5</sup>

## AFFILIATIONS

<sup>1</sup>Lawrence Livermore National Laboratory, Livermore, California 94550, USA

<sup>2</sup>Los Alamos National Laboratory, Los Alamos, New Mexico 87545, USA

<sup>3</sup>Massachusetts Institute of Technology, Cambridge, Massachusetts 02139, USA

<sup>4</sup>General Atomics, San Diego, California 92121, USA

<sup>5</sup>Diamond Materials GmbH, Freiburg 79108, Germany

**Note:** This paper is part of the Special Collection: Papers from the 64th Annual Meeting of the APS Division of Plasma Physics.

**Note:** Paper G11 3, Bull. Am. Phys. Soc. **67** (2022).

<sup>a)</sup>Invited speaker.

<sup>b)</sup>Author to whom correspondence should be addressed: do6@llnl.gov

## ABSTRACT

While nuclear fusion ignition has been achieved at the National Ignition Facility in inertial confinement fusion (ICF) experiments, obtaining higher gain and more efficient burn is still desired. In that regard, increasing the compression of the fuel is an important factor. In recent indirect-drive capsule implosions, the SQ-n campaign is testing the hypothesis that reducing the hydrodynamic growth of perturbations is key to achieving higher compression of high-density carbon based-ablators for ICF. SQ-n uses a design at lower adiabat with a ramped foot laser pulse shape to minimize early-time hydrodynamic instability growth, predicted to be reduced by a factor of 10, and an optimized ablator dopant distribution. Subsets of experiments were conducted within the SQ-n campaign to study the implosion symmetry, laser backscatter, stability, and compression. Only the latter two will be reviewed here. Shock timing experiments using the velocity interferometer system for any reflector diagnostic enabled the development of a gently accelerating shock velocity. The ice-ablator interface acceleration, important for managing the Richtmyer–Meshkov phase growth, was observed with refraction enhanced radiography and the ablation front growth was measured using radiography of pre-imposed modulations. Finally, layered tritium-hydrogen-deuterium ( $\sim 75\%$  H,  $\sim 25\%$  T,  $\sim 2\text{--}10\%$  D) and deuterium–tritium implosions demonstrate that between  $15\% \pm 3\%$  and  $30\% \pm 6\%$  improved compression has been achieved.

Published under an exclusive license by AIP Publishing. <https://doi.org/10.1063/5.0167424>

## I. INTRODUCTION

Indirect-drive inertial confinement fusion (ICF)<sup>1–5</sup> experiments are imploding capsules at the National Ignition Facility (NIF)<sup>1</sup> using the facility's 192 laser beams with up to 2.1 MJ of energy, with the goal of reaching thermonuclear ignition and high gain. The laser energy is converted to thermal x rays inside a high-Z cavity (*Hohlraum*) and an  $\sim 1$  mm radius capsule (ablator) is filled with an ice layer of

deuterium–tritium (DT) fuel and is ablated by the x rays, causing the capsule to implode, compress and heat the DT, and ignite. A capsule's inner layer doped with a mid-to-high-Z material shields the ice-ablator interface from hard x-ray preheat, required to maintain high fuel compression.<sup>6</sup>

Recent implosions using high density carbon (HDC) diamond capsules have achieved record fusion yields in the burning plasma

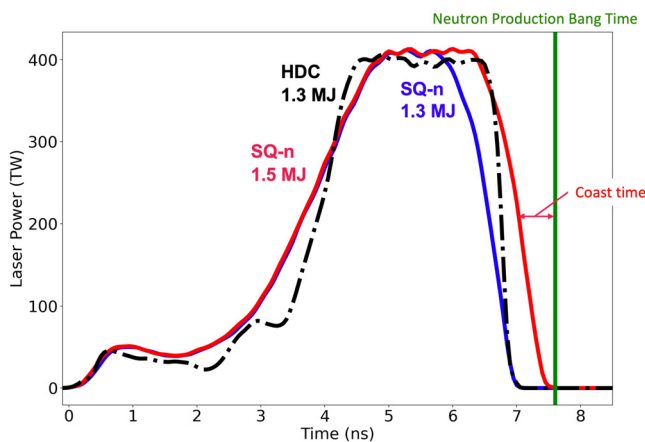
regime.<sup>7–9</sup> Still, the fusion yields and compression performances are below what was expected from hydrodynamic simulations.<sup>10,11</sup> Increasing the compression of the DT ice fuel during stagnation is essential for increasing fuel burnup and hence achieving multi-megajoule yields in ICF implosions. One hypothesis for the performance degradation is the lower compression due to fuel–ablator mixing.<sup>12</sup>

A typical three-shock implosion uses an HDC ablator and is called here the “HDC design.”<sup>13,14</sup> A sample of the laser pulse drive for such an implosion is presented in Fig. 1 in a black dashed-dotted line. When the laser pulse starts its rise and reaches the first step at around 1 ns, it will launch a shock that is traveling through the ablator. When it reaches the ablator–fuel interface, the latter is set in motion at constant velocity. The following two steps in the laser pulse, at 3 and 4 ns, launch new shocks that are timed to all merge at the DT fuel–gas boundary. Any shock that leaves a fuel–ablator interface with constant velocity leads to an inherently linearly growing perturbation growth due to the Richtmyer–Meshkov (RM) instability<sup>15–17</sup> that are seeds of the Rayleigh–Taylor (RT)<sup>18,19</sup> instability during the subsequent acceleration phase.<sup>20,21</sup> Being able to control these instabilities is key to improving the stability throughout the implosion and limit the ablator mix at the ice–ablator interface; this motivated the development of the SQ-n design (“S” for scaling and “Q” for quality).

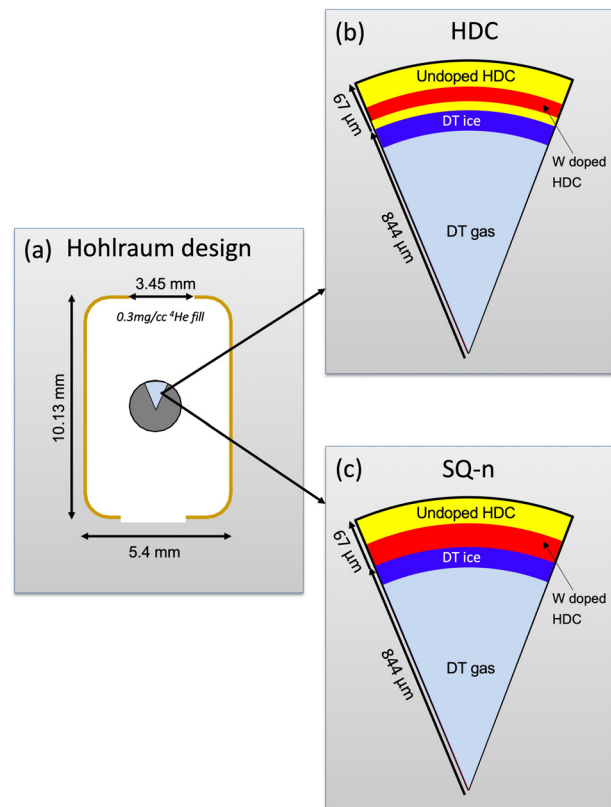
The SQ-n design goal is to achieve higher DT fuel compression<sup>22–26</sup> while controlling instabilities. To that effect, the SQ-n design uses a ramp in the foot of the laser pulse from 2 to 5 ns as shown in Fig. 1 by the red and blue curves, to drive an accelerating first shock through the ablator. The compression wave is then launched to merge with the first shock just inside the DT fuel–ablator boundary. The accelerating shock will impose a steady acceleration of the fuel–ablator interface and is predicted to replace RM growth with stable RT oscillations as shown in Ref. 26. The second key concept for the SQ-n campaign is the reduction of the number of interfaces in the capsule ablator. The current designs use a *Hohlraum* with the capsule placed at its center [Fig. 2(a)]. The HDC campaign uses a buried dopant layer inside the undoped ablator layer<sup>7–9</sup> [Fig. 2(b)]. The SQ-n design now uses a tungsten (W) doped inner layer all the way to the ice, a so-called

“W-inner” dopant [Fig. 2(c)]. The reason for traditional ICF capsule design used buried layer is that the W-doped HDC layer absorbs a significant fraction of the hard x-ray pre-heat from the *Hohlraum* causing this layer to heat up and therefore be less dense at the same pressure. The inner undoped region absorbs less pre-heat, however, and so remains cold and dense with a better density match to the even colder DT fuel. This closer density match makes for a more stable interface and limits RT growth at the fuel–ablator interface. However, it has been realized that the un-doped to doped transition inside the ablator produces a quite unstable interface of its own that can substantially increase ablator–fuel mixing.<sup>23</sup> Removing this interface and increasing the net amount of dopant to still maintain density match to the DT is the motivation for moving to a W-inner dopant profile. Thus, reducing the number of interfaces decreases the region where the hydrodynamic instabilities can develop. This, combined with the accelerating first shock, is expected to result in a better overall capsule stability.<sup>23,26</sup>

All experiments are done with “sub-scale” capsules with a ~25% reduced size compared to the “full-scale” experiments that achieved ignition on NIF. This was done as a cost-efficiency method for the first phase of the campaign development. Reducing the implosion scale impacts the instability evolution due to the fixed scale length of the ablation front. For a given x-ray drive spectrum and capsule dopant concentration, the x-ray attenuation length in the ablator is a fixed physical length scale. As the capsule is scaled down, therefore, this



**FIG. 1.** Laser pulse shape of the drive used in HDC (black dashed-dotted line) and SQ-n (plain red and blue lines) capsule implosion experiments. The coast time is defined as the time between half of the laser turn-off and the peak neutron production time, or bang time (BT).



**FIG. 2.** (a) Schematic of the target design for ICF capsule implosion experiments. (b) Buried layer doped capsule for the HDC design; and (c) the inner layer doped capsule for the SQ-n design. The capsule is placed at the center of a *Hohlraum*.

14 November 2023 19:19:28

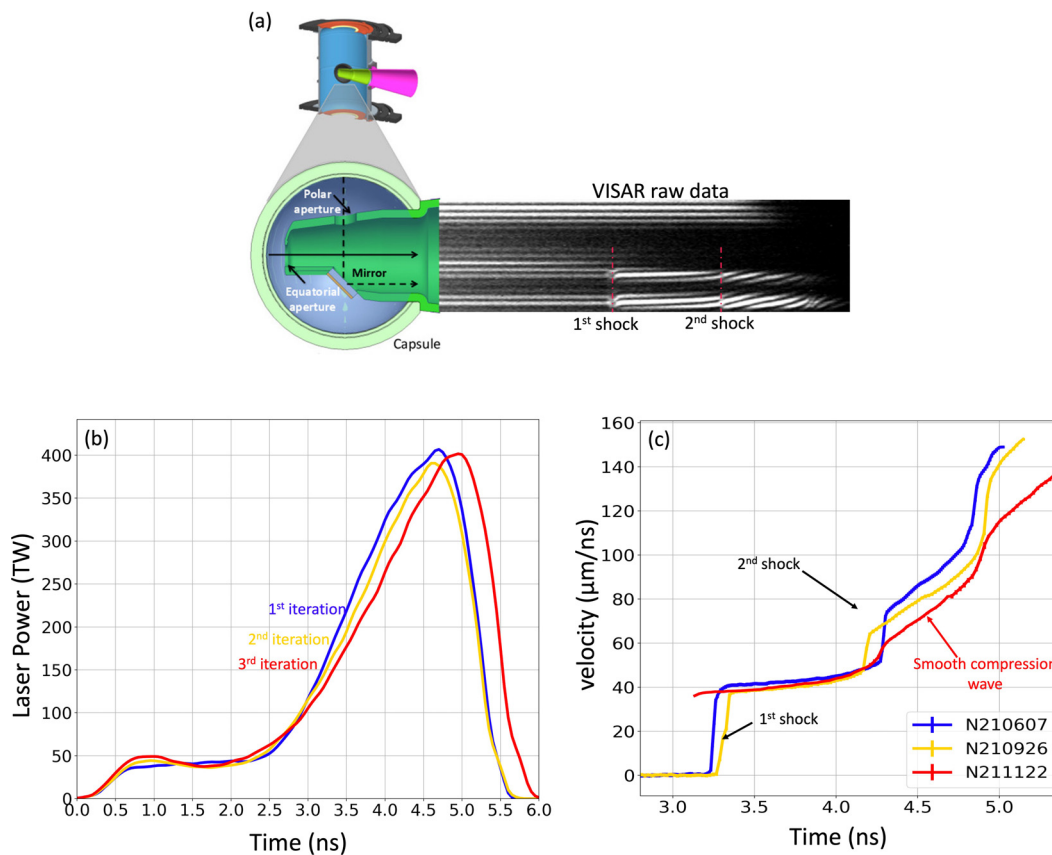
fixed attenuation length does not scale, and the density scale length of the ablation front becomes proportionately larger at subscale than full scale. This makes sub-scale implosions relatively more stable at the ablation front than their full-scale counterparts. For the same reason, sub-scale capsules also require higher dopant concentrations if they are to attenuate the same number of hard x-rays in a scaled down dopant layer. Another consequence is the reduced laser backscatter down to a noise level in these types of experiments; future full-scale experiments will allow a more in-depth study of laser backscatter.

The sub-scale SQ-n experimental campaign is using existing experimental platform to demonstrate each of the design points that is predicted to improve capsule implosion compression in the simulations at NIF.<sup>23</sup> The experimental results of the campaign first phase are reviewed in this paper. The first step is the design of the laser drive to obtain a single accelerating shock compression; the stability measurements are done through the measurement of the ice–ablator interface and the ablation front growth rate; finally, the compression quality is measured during layered DT capsule implosion.

## II. LASER DRIVE DESIGN

A key concept behind the SQ-n design is that it only has a single shock in the RM phase, followed by a smooth compression wave rather than multiple successive shocks. To achieve such smooth shock evolution, we used the keyhole platform.<sup>27</sup> In these experiments, a liquid deuterium–deuterium (D2) filled capsule replaces the traditional DT ice fuel inside the *Hohlraum* and is imploded using the full 192 NIF beams. As only the RM phase and the start of the acceleration phase is of interest, the laser pulse has been truncated just after reaching the peak power to limit optics damage to the NIF laser system.

An imaging cone [Fig. 3(a)] opens a line of sight to a velocity interferometer system for any reflector (VISAR) diagnostic that measures the shock velocity inside the capsule shell through interferometry; details on the diagnostic and data analysis is given in Ref. 28. The first iteration of the pulse design used slightly increased picket (first laser pulse step) power compared to the three-shock HDC design as well as a ramped rise [blue curve on Fig. 3(b)]. This results in a slight acceleration after the first shock breakout, between 3.3 and 4.3 ns [Fig. 3(c) plain blue]. A strong second shock catch-up event is still



**FIG. 3.** (a) The shock-timing keyhole platform enables the direct measurement of the sequence of shock waves launched into an indirectly driven capsule. A gold cone inserted into the capsule and a turning mirror open two lines of sight for the line-imaging VISAR, which tracks the velocity of the leading shock front in cryogenic liquid D2 along the equatorial (90–315) direction.<sup>26,29</sup> (b) Starting from a three-shock design, incremental changes to the laser pulse picket power slope of the rise to peak power have been applied for the VISAR experiments. (c) Leading shock velocity history in the liquid D2 determined from the VISAR signal along the equator of the capsule. While the first and second iterations of the laser pulse induce a series of shock waves, with a distinct velocity jump when the second shock catches up to the first shock, the third iteration of the pulse shape (red) produces a shock wave with the desired continuously increasing velocity up to ~4.8 ns.

present at around 4.35 ns and needs to be smoothed out. The second and third iteration of the experiments increased progressively the picket pulse and the ramp to the peak power duration, with each iteration seeing a higher shock acceleration after the first shock reduced acceleration upon 1–2 shock catch ups. The final design [Fig. 3(c) plain red] shows a continuously increasing leading shock during the RM phase as desired, note that the first shock is truncated due to lower data quality on this shot. A later second shock can be observed around 4.9 ns and is due to a reverberation of the shell as the release wave from the first shock breakout rebounds from the ablation front in a so-called  $N + 1$  shock. This smooth shock evolution is predicted to make the fuel–ablator interface accelerate as required. The velocity measurement is consistent with the calculated value of low-adiabat of about  $\sim 3$  for the SQ-n drive.<sup>23</sup> This achieves the goal of keeping an adiabat close to the previous HDC sub-scale design of 2.6 and far from the higher adiabat sub-scales “Big-Foot” (BF)<sup>30,31</sup> at 4.6–4.7.

### III. STABILITY MEASUREMENT

One of the core mechanisms predicted to reduce the compression performance in ICF implosions is the hydrodynamic instability growths that are generated at the different interfaces and produce material mixing. Three main mixing regions can be identified: the ablation front instability, the fuel–ablator interface instability, and the hotspot instability. Measuring and controlling the mixing is key to improving the stability throughout the implosion. In this paper, we are focusing on the ablation front and the fuel–ablator interface, the hotspot instability measurement platform being under development.

#### A. Fuel–ablator interface acceleration

A key feature of the SQ-n design is to achieve continuous acceleration of the fuel–ablator interface that is predicted to result in an early-time oscillation of the instability seeds and thus improve stability. It has been designed to create a 10–20  $\mu\text{m}/\text{ns}^2$  acceleration of the DT fuel–ablator interface after the first shock. The initial Atwood number ( $A$ ) at that interface,  $A = (\rho_{\text{ablator}} - \rho_{\text{fuel}}) / (\rho_{\text{ablator}} + \rho_{\text{fuel}})$  is stable (negative). Early time, before the second shock breakout, the instability seeds are predicted to be on the order a micrometer or less, even for the more unstable HDC design.<sup>26</sup> Such a small scale is not measurable *in situ* but can be inferred with simulation. Figure 4 presents the simulation of the evolution of the growth factor for a 1  $\mu\text{m}$  wavelength for the HDC (red) and SQ-n (blue) drive using the Hydra code.<sup>32</sup> When the ice–ablator interface is not accelerating during the shock propagation phase, the perturbation experiences RM growth linear in time (red). Now, in the presence of an acceleration of the ice–ablator interface, the growth of simultaneous RT instabilities appears. Rather than a linear growth, the resulting growth factor is now predicted to be oscillating (blue line).<sup>26</sup> The growth equation for the instability at a time  $t$  in this case is

$$h(t) = h_0 \cos(\gamma t) + \frac{h_0}{\gamma} \sin(\gamma t).$$

With  $h_0$  the initial perturbation amplitude, and  $\gamma = Agk$ , with  $g$  the acceleration and  $k$  the wave number. The initial growth rate for the RM being  $h_{0, \text{RM}} = \Delta V A k h_0$  with  $\Delta V$  the velocity jump at the interface caused by the shock. This results that the RM have a maximum amplitude of  $h_0 \sqrt{1 + \Delta V^2 A k^2 / g}$ . This leads to a decrease in the

Growth factor for 1  $\mu\text{m}$  wavelength perturbation

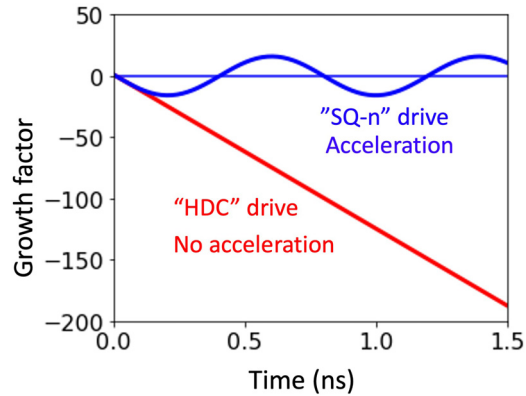


FIG. 4. Simulation using the Hydra hydrodynamic code<sup>32</sup> of the growth factor evolution for 1- $\mu\text{m}$  wavelength perturbation in the case without ice–ablator interface acceleration like with HDC drive (red) and with ice–ablator interface acceleration with the SQ-n drive (blue). In the presence of an accelerating interface, the growth factor will oscillate rather than grow linearly which will limit the seeds of instability for later time.

perturbation growth during the shock propagation phase and will reduce the instability seeds for the subsequent RT phase. A direct consequence is the reduction of mixing during peak compression (stagnation). If the oscillation is slow (small mode number) then the growth is the same as RM-only, so this stabilizing mechanism is only helpful for fine-scale features like HDC microstructure. The main concern at this interface is mixing seeded by the 100 nm–1  $\mu\text{m}$  scale grains,<sup>33</sup> which is why this stabilization mechanism is expected to be helpful.

To measure the ice–ablator interface acceleration during the RM phase, we used refraction enhanced radiography (RER).<sup>24,34–36</sup> This platform consists of a one-dimensional x-ray point projection imaging with a 5  $\mu\text{m}$  slit and a zinc (Zn) foil backlighter, producing 9 keV photons as the source as shown in Fig. 5. This imaging system is used to radiograph the limb of a capsule that is imploded inside a *Hohlraum* using the SQ-n drive. The refraction at the density gradients of the limbs is used to improve the imaging contrast compared to classic absorption.<sup>37</sup> This system yields a one-dimensional x ray, time-resolved image over 2 ns with about 6- $\mu\text{m}$  spatial and 100-ps temporal resolution. RER is used on an ICF shot with a tritium–hydrogen–deuterium (75% H, 24.2% T, 0.8% D) ice layer inside a undoped

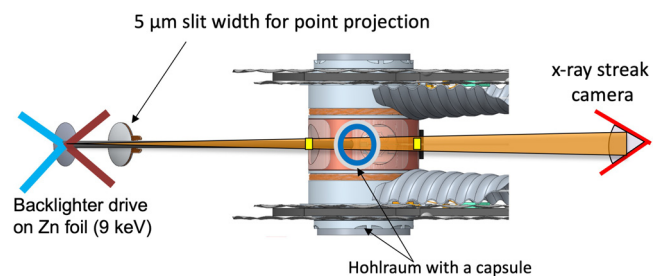


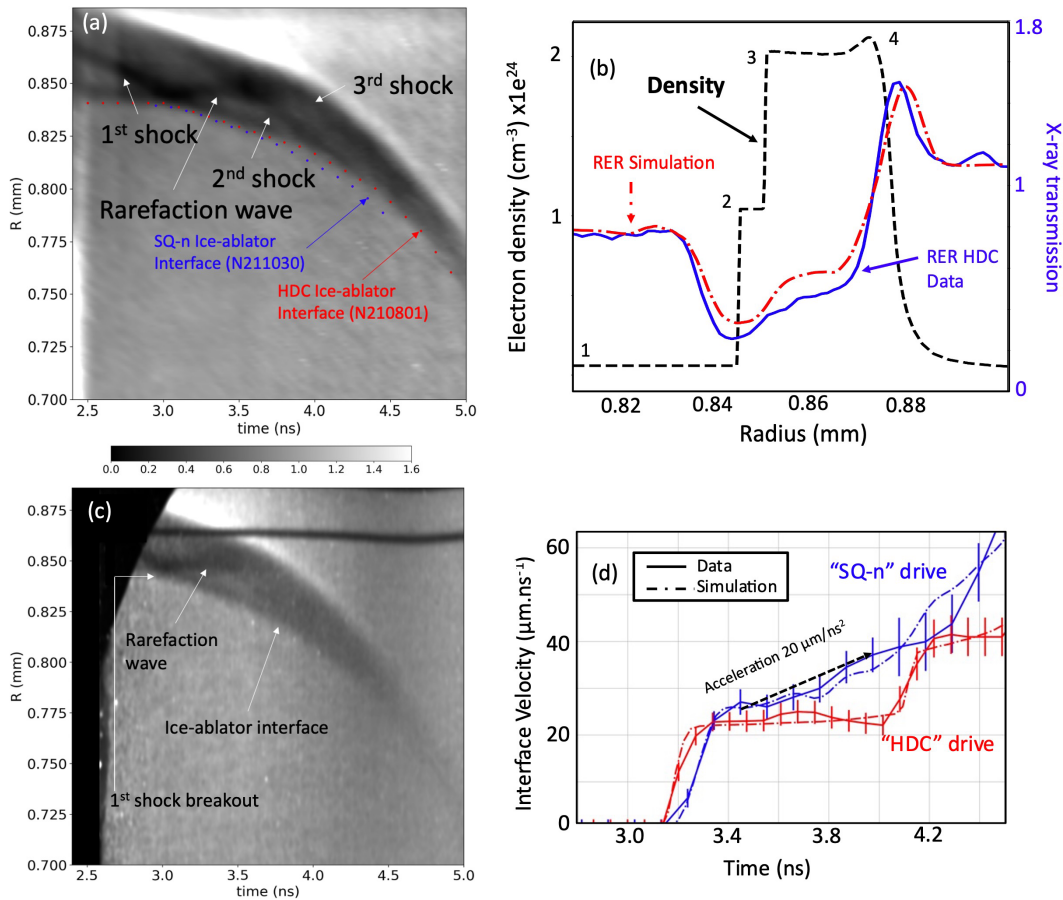
FIG. 5. Refraction enhanced radiography (RER) experimental set-up. An ICF implosion target is radiographed using a point projection method. The x-ray backlighter is a Zn foil driven by 16 NIF beams and down-selected to a line using a 5- $\mu\text{m}$  slit.



capsule using 160 NIF beams to drive a gold *Hohlraum* with 1.015 MJ total energy, 14 NIF beams are used for generating the x-ray back-lighter and 18 NIF beams were turned off for symmetry or geometrical purpose as presented in Ref. 24. Because less beams were used to generate the *Hohlraum* drive, an energy compensation proportionate to the loss of the 32 beams has been applied to the remaining 160 beams. An asymmetry is expected to occur in the slit-x-ray streak camera axis perpendicular to the RER probed limb region and thus is expected to have less impact on the measurement. The capsules used in the experiments are undoped to increase the RER image contrast. While this difference would result in a light difference in shock velocities, the overall behavior of the ice–ablator interface is unchanged and allows relevant comparison between different drive designs.

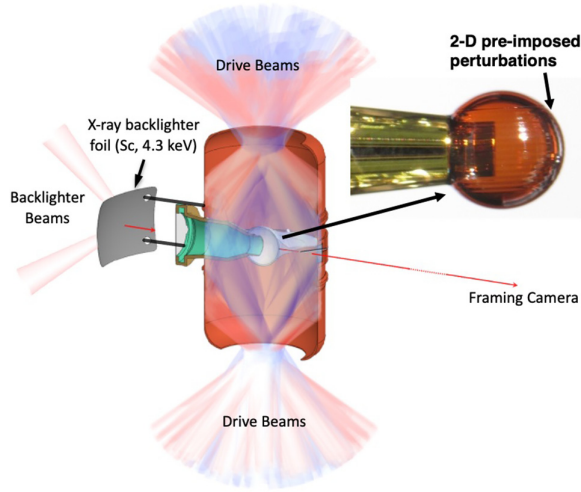
Figures 6(a) and 6(c) show the measured streaked 1D radiographs using the previously described RER platform for an HDC type implosion (a) and SQ-n type implosion (c). They can be read as a shock plot with the time on the x-axis, the capsule radius on the y-axis and the x-ray intensity as the grayscale. From a radius of 0.7

to 0.84 mm is the fuel, including the ice layer; the dark region between 0.844 and ~0.880 mm is the capsule ablator; and after that is the outside of the capsule. Inside the ablator, three shocks and the rarefaction wave are clearly visible for the HDC case, whereas the SQ-n has only one shock and a rarefaction wave. A lineout of a simulated RER along with the absorption and density is presented on Fig. 6(b). Region 1 is the fuel, region 2 is the fuel–ablator interface, region 3 is the first shock front, and region 4 is the ablation front. Looking at the RER in plain red, it has high-contrast refraction fringes for all interfaces, allowing a precise measurement of the evolution of the interfaces. The data obtained in the case of the HDC drive [shown in Fig. 6(a)] show very good agreement with the simulation, as presented on a RER as lineout on Fig. 6(b) in plain blue, with the shocks and the rarefaction wave visible; the ice–ablator interface is also very well delimited, which allows the measurement of the interface trajectory. The same measurement was performed for the SQ-n drive [Fig. 6(c)],<sup>24</sup> and the interface velocity comparison is shown on Fig. 6(d). It is shown that after each subsequent shock, the HDC drive sees no acceleration of the



**FIG. 6.** (a) and (c) Experimental data<sup>24</sup> of the RER signal for the HDC and SQ-n designs, respectively. The HDC design shows traces inside the ablator for the first, second, and third shocks whereas the SQ-n shows traces of the first shock and a very faint second shock when the rarefaction wave is reflected onto the ablation front. (b) Line out of the simulated density profile for an HDC implosion (black dashed) at 2.8 ns showing the different density gradients due to the interface in comparison with simulated RER (red dashed-dotted) expected x-ray transmission and data from RER shot (blue plain) from (a). (d) Measured and simulated ice–ablator interface velocity for the SQ-n (blue) and HDC (red) drive as presented in Ref. 24. (a), (c), and (d) reproduced with permission from Do *et al.*, Phys. Rev. Lett. **129**, 215003 (2022). Copyright 2023 American Physical Society.

14 November 2023 19:19:28



**FIG. 7.** Experimental configuration for the HGR platform. An HDC capsule with 2D pre-imposed perturbations, and an imaging cone is placed inside a *Hohlraum*. The backlighter consist of a scandium (Sc) foil generating 4.3 keV photons to radiograph the perturbation growth. A framing camera is used to record the images at four different times.

ice–ablator interface as the velocity is flat. On the other hand, the SQ-n drive has a smooth acceleration of the interface after the first shock of  $20 \mu\text{m ns}^{-1}$  as shown by the black dashed line on Fig. 6(d). This value is as predicted by the simulation and should reduce the hydrodynamic instability seeds and improve stability throughout the implosion. Note that the SQ-n data on Fig. 6(c) displays a pinching after 4 ns which is caused by the saturation of the camera, resulting in the larger error bar of the velocity on Fig. 6(d). An explanation for the discrepancy with simulation at this time is the drive difference at later time due to turned off and backlighter NIF beams in the experiment while doing the simulations with all NIF beams as drivers.

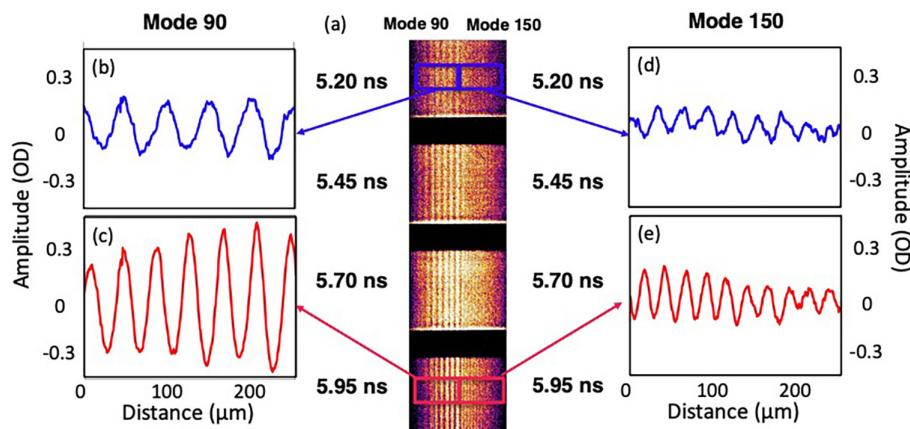
**B. Ablation front growth rate**

The SQ-n design is based on keeping similar stability as a previous design called Big-Foot<sup>30,31</sup> while working at lower adiabat.

To verify this stability hypothesis, the hydro-growth radiography (HGR) platform<sup>38</sup> has been used to measure the ablation front areal-density growth and compare it to previous designs. In this experiment, 2D perturbations are pre-imposed on an HDC capsule shell (Fig. 7). To allow comparison with previous experiments, mode 90 and mode 150 ( $\lambda_0 = 64$  and  $38 \mu\text{m}$ , respectively) were chosen. Ideally, a mode number close to the peak growth factor, around mode 60, the measurement becomes more challenging as less good quality cycles are radiographed due to the higher wavelength. The mode 150 serves as control point as it usually converges toward the “zero-nod.”

The temporal evolution of the perturbations is measured using 1D radiography. The resolution is set by the  $10\text{-}\mu\text{m}$ -wide slit and the backlighter energy by the foil material (scandium, Sc, 4.3 keV). The image is recorded on a four-strip framing camera with each strip triggering at a different time [Fig. 8(a)]. Figures 8(b) and 8(c) and Figs. 8(d) and 8(e) show lineouts of the optical density amplitude for the first and last time of the mode 90 perturbations and mode 150, respectively. The amplitudes grow as wavelengths are decreasing throughout the implosion. The measurement of the optical density amplitude allows the calculation of the areal density ( $\rho R$ ) amplitude. It can then be divided by the initial areal density ( $\rho_0 R_0$ ) to obtain the areal density growth factor (dimensionless).<sup>39</sup>

The metric used for comparison with previous experiments is the radii convergence ratio ( $C_r$ ), defined as the ratio of the capsule radius (at ablation front) at the considered time over the initial radius,  $R_0$ . Figure 9 presents the areal density growth factor for different implosion designs at a convergence ratio of 1.5.  $C_r$  1.5 is close to the saturation limit of the growth of initial large amplitude perturbation in our ablator and representative of the measured  $C_r$  range in our experiments. Early ICF experiments at NIF used a depleted uranium *Hohlraum* (red squares); its lower M-band x-ray emission reduces x-ray preheat of the ablator and requires less ablator doping.<sup>40</sup> It was then realized that having this lower M-band preheat is reducing the constraint applied on the ablation front hydrodynamic instabilities, leading to accrue growth factor and thus more instable interface. The following campaigns, named HDC and Big-Foot (BF), used gold *Hohlraum* designs obtaining better growth factor (light blue diamonds and green circles). The growth factor at mode 150 is very sensitive when approaching the zero-nod so it is not surprising that for some measurement a certain level of discrepancy is observed relative to the



**FIG. 8.** (a) Images of the perturbations at four different times. Lineouts of the mode 90 and mode 150 perturbations at the first (b) and (d), respectively, and last (c) and (e), respectively, time step are displayed.

14 November 2023 19:19:28

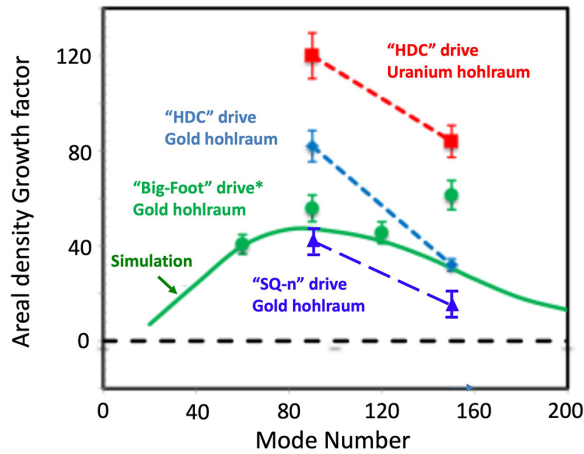


FIG. 9. Comparison of the measured areal density growth factor for different drives at a  $C_r$  1.5: HDC drive with different *Hohlraum* material (red square, light blue diamond); Big-Foot (green circle); and SQ-n drive (dark blue triangle).

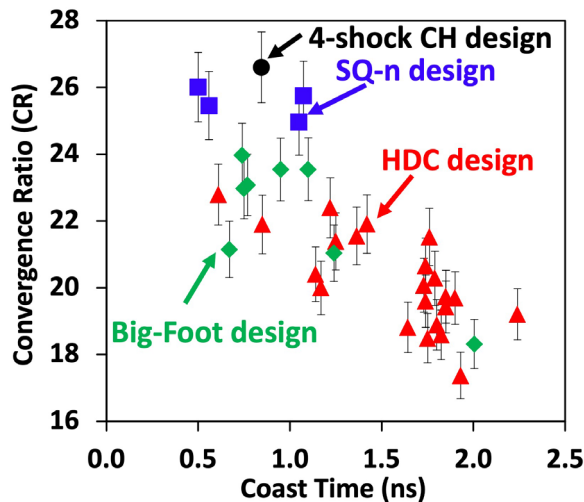


FIG. 10. Measured convergence ratio relative to the coast time for the HDC drive (red triangle), the Big-Foot drive (green diamond), the four-shock CH drive (black circle), and the SQ-n drive (blue square).

simulations. As previously stated, one of the goals of the SQ-n design is to reach lower adiabat than the BF campaign while keeping a similar ablation front stability. As a comparison, we displayed BF simulated growth factor at  $C_r$  1.5 with a maximum around mode 80.

The measurements show that the SQ-n growth factor measurements are low and close to the BF ones as expected. It implies that the ablation front stability has been conserved with this new design.

IV. IMPROVED COMPRESSION MEASUREMENT

The step after the drive design and the interface stability measurements is to measure the resulting capsule compression for SQ-n through capsule implosion experiments. The compression is inferred through the fuel areal density,  $\rho R$ , that is directly related to the down scatter ratio (DSR).<sup>41</sup> The latter is measured by the neutron time-of-flight (nTOF) diagnostic<sup>42</sup> on NIF. A detailed comparison and discussion about the DSR of the SQ-n campaign is presented in Ref. 25. In this paper, to compare normalized values over the different campaigns, the compression ratio (CR) is used as a criterion for capsule compression quality and is defined as<sup>43</sup>

$$CR = \sqrt{\frac{(\rho R)_{BT}}{(\rho R)_0}}$$

with  $(\rho R)_{BT}$  the fuel areal density at the peak neutron emission or bang time (BT) and  $(\rho R)_0$  the fuel initial areal density. This quantity is insensitive to capsule dimension and fuel ice thickness and allow a fair comparison between the experiments.

The SQ-n implosion used the new W-inner capsule design presented in Fig. 2 with a 0.4% W-doped inner layer in the ablator placed inside a gold (Au) *Hohlraum* (10.13 mm length, 5.40 mm diameter, 3.45 mm laser entrance hole size). The fuel used in these experiments was either tritium–hydrogen–deuterium (75% H, 24.2% T, 0.8% D) or deuterium–tritium (50% D, 50%T). A  $\sim 43\text{-}\mu\text{m}$  ice layer is formed at the interface with the ablator. In these experiments, 192 NIF beams drove the *Hohlraum* with either 1.3 or 1.5 MJ. The energy was gradually increased to reduce coast time. Previous NIF sub-scale capsule implosion campaigns<sup>44–46</sup> have shown a very strong correlation between the CR and the coast time, defined as the time between half of the laser drive turn-off and BT. Reducing coast time will reduce the radius at peak velocity with the effect of increasing the energy transfer from the implosion kinetic energy to the hotspot energy.

The CR measurements are plotted against the coast time on Fig. 10 for four different drives; the shot data summary is presented in Table I. The HDC and BF measurements follow the same linear trend of CR vs coast time. On the other hand, the SQ-n CR measurements were higher for the same coast time. The highest SQ-n CR is tied with the higher adiabat “four-shock CH” campaign<sup>5,47</sup> for the highest CR ever measured on NIF capsule implosion experiments. The four-shock CH design relied on low adiabat ( $\sim 1.6$ ) but has proven to be very unstable and underperformed both in terms of predicted yield and compression.<sup>48</sup> On the other hand, the SQ-n design, while having a

TABLE I. DT and tritium-hydrogen-deuterium (THD) ( $\sim 25\%$  T,  $\sim 75\%$  H,  $\sim 2\text{--}10\%$  D) SQ-n campaign shot data breakdown of coast time, convergence ratio, neutron yield, and ion temperature.

Shot name	Shot type	Coast time (ns)	CR	Neutron yield	Tion (keV)
N220115-001-999	THD	1.07	$25.8 \pm 1.03$	$6.54 \times 10^{13} \pm 1.6 \times 10^{12}$	$3.99 \pm 0.13$
N220320-002-999	DT	1.05	$25.0 \pm 1.00$	$4.43 \times 10^{15} \pm 1.2 \times 10^{14}$	$4.03 \pm 0.13$
N220501-003-999	THD	0.5	$26.0 \pm 1.04$	$5.80 \times 10^{13} \pm 2.0 \times 10^{12}$	$3.84 \pm 0.13$
N220604-001-999	DT	0.56	$25.5 \pm 1.02$	$6.61 \times 10^{15} \pm 1.8 \times 10^{14}$	$4.32 \pm 0.19$

14 November 2023 19:19:28



higher adiabat ( $\sim 3$ ) increased stability and is expected to get better yield. While shot to shot variation of  $\sim 5\%$  is present as shown by BF and HDC points, the SQ-n points display higher CR than any other equivalent shot at a coast time around 1.1 ns. Comparing to BF shots, this is a  $13\% \pm 4\%$  improvement in CR. This net increase was predicted by simulations in Ref. 23 where 15.8% better compression performances was expected from SQ-n with relative to BF in the same condition. This support the fact that the compression improvement is mainly due the improvement of stability by the SQ-n design. Overall, the SQ-n has improved compression between  $15\% \pm 3\%$  and  $30\% \pm 6\%$  for the same coast time compared to similar experiments, which is very promising and will lead to a higher yield amplification than the 1.4 MJ record previously mentioned.

## V. SUMMARY AND CONCLUSION

In conclusion, a new indirect ICF drive called SQ-n has been designed to improve compression performance by increasing stability throughout the drive. This paper reports on the experimental campaign that demonstrated the key hypotheses of this new design: (1) a smooth compression wave replacing the second and third shocks in the drive induces an acceleration of the ice–ablators interface during the RM phase and (2) a W-inner-type doped capsule will increase stability throughout the implosion. The measurements showed that the stability in the SQ-n design was controlled throughout the implosion. This led to an improvement of  $15\% \pm 3\%$  to  $30\% \pm 6\%$  in capsule compression. The next step will be to confirm the lower amount of hot and cold mix using a high-spatial and energy resolution x-ray imager. Following this measurement, the design will be improved to reach a lower adiabat of around 2.5 and begin ramping up to full-scale experiments to increase the yield.

## ACKNOWLEDGMENTS

The authors would like to acknowledge NIF Target Fabrication and Facility and Operations for help in fielding these experiments. This work was performed under the auspices of the U.S. Department of Energy by Lawrence Livermore National Laboratory under Contract Nos. DE-AC52-07NA27344 and LLNL-JRNL-847847.

## AUTHOR DECLARATIONS

### Conflict of Interest

The authors have no conflicts to disclose.

### Author Contributions

**Alexandre Do:** Data curation (equal); Formal analysis (equal); Investigation (equal); Writing – original draft (lead); Writing – review & editing (lead). **Daniel T. Casey:** Conceptualization (equal); Data curation (equal); Formal analysis (equal); Investigation (equal); Project administration (lead); Writing – original draft (supporting); Writing – review & editing (supporting). **Daniel S. Clark:** Conceptualization (equal); Data curation (equal); Formal analysis (equal); Investigation (equal); Project administration (lead); Writing – original draft (supporting); Writing – review & editing (supporting). **Benjamin Bachmann:** Data curation (equal); Formal analysis (equal); Investigation (equal). **Kevin Baker:** Data curation (equal); Formal analysis (equal); Investigation (equal). **Tom Braun:** Resources (equal). **T. Briggs:** Resources (equal). **Thomas Chapman:** Resources (equal). **Peter M. Celliers:** Data curation (equal); Formal analysis (equal);

Investigation (equal). **Hui Chen:** Data curation (equal); Formal analysis (equal); Investigation (equal). **C. Choate:** Resources (equal). **Eduard Liviu Dewald:** Data curation (equal); Formal analysis (equal); Investigation (equal); Writing – original draft (supporting); Writing – review & editing (supporting). **Laurent Divol:** Conceptualization (equal); Investigation (equal). **Gilda fathi:** Resources (equal). **David N. Fittinghoff:** Data curation (equal); Formal analysis (equal); Investigation (equal). **Gareth Neville Hall:** Data curation (equal); Formal analysis (equal); Investigation (equal). **Edward Paul Hartouni:** Conceptualization (equal); Formal analysis (equal); Investigation (equal). **Dean Marcu Holunga:** Resources (equal). **Shahab Firasat Khan:** Data curation (equal); Formal analysis (equal); Investigation (equal). **A. L. Kritcher:** Investigation (equal); Supervision (equal). **Otto L. Landen:** Investigation (equal); Supervision (equal); Writing – original draft (supporting); Writing – review & editing (supporting). **Andrew MacPhee:** Data curation (equal); Formal analysis (equal); Investigation (equal). **Marius Millot:** Data curation (equal); Formal analysis (equal); Investigation (equal); Writing – original draft (supporting); Writing – review & editing (supporting). **Edward Marley:** Data curation (equal); Formal analysis (equal); Investigation (equal). **Jose L. Milovich:** Formal analysis (equal); Investigation (equal). **Abbas Nikroo:** Resources (equal). **Arthur Pak:** Investigation (equal); Project administration (equal); Supervision (equal). **David J. Schlossberg:** Data curation (equal); Formal analysis (equal); Investigation (equal). **V. A. Smalyuk:** Investigation (equal); Project administration (equal); Supervision (equal); Writing – original draft (equal); Writing – review & editing (equal). **Michael Stadermann:** Resources (equal). **David J. Strozzi:** Data curation (equal); Formal analysis (equal); Investigation (equal). **Riccardo Tommasini:** Data curation (equal); Formal analysis (equal); Investigation (equal). **Christopher Weber:** Conceptualization (equal); Formal analysis (equal); Investigation (equal). **Brandon Woodworth:** Project administration (equal). **Dexter Yanagisawa:** Resources (equal). **Noah W. Birge:** Data curation (equal); Formal analysis (equal). **Christopher R. Danly:** Data curation (equal); Formal analysis (equal). **Mora Durocher:** Data curation (equal); Formal analysis (equal). **Matthew S. Freeman:** Data curation (equal); Formal analysis (equal). **Hermann Geppert-Kleinrath:** Data curation (equal); Formal analysis (equal). **Verena Geppert-Kleinrath:** Data curation (equal); Formal analysis (equal). **Yongho Kim:** Data curation (equal); Formal analysis (equal). **Kevin Meaney:** Data curation (equal); Formal analysis (equal). **Carl Wilde:** Data curation (equal); Formal analysis (equal). **Maria Gatu Johnson:** Data curation (equal); Formal analysis (equal). **Anthony Allen:** Resources (equal). **Mark Ratledge:** Resources (equal). **Casey Kong:** Resources (equal). **Tobias Fehrenbach:** Resources (equal). **Christoph Wild:** Resources (equal).

## DATA AVAILABILITY

The data that support the findings of this study are available from the corresponding author upon reasonable request.

## REFERENCES

- G. H. Miller, E. I. Moses, and C. R. Wuest, “The National Ignition Facility: Enabling fusion ignition for the 21st century,” *Nucl. Fusion* **44**, S228 (2004).
- J. Lindl, “Development of the indirect-drive approach to inertial confinement fusion and the target physics basis for ignition and gain,” *Phys. Plasmas* **2**(11), 3933 (1995).

- <sup>3</sup>S. Atzeni and J. Meyer-ter-Vehn, *The Physics of Inertial Fusion: Beam Plasma Interaction, Hydrodynamics, Hot Dense Matter* (Oxford University Press, Oxford, 2004).
- <sup>4</sup>E. I. Moses, J. Atherton, L. Lagin, D. Larson, C. Keane, B. MacGowan, R. Patterson, M. Spaeth, B. Van Wonerghem, P. Wegner *et al.*, “The National Ignition Facility: Transition to a user facility,” *J. Phys.: Conf. Ser.* **688**, 012073 (2016).
- <sup>5</sup>J. D. Lindl, O. L. Landen, J. Edwards, E. I. Moses, J. Adams, P. A. Amendt, N. Antipa, P. A. Arnold, R. C. Ashbranner, L. J. Atherton *et al.*, “Review of the National Ignition Campaign 2009–2012,” *Phys. Plasmas* **21**, 020501 (2014).
- <sup>6</sup>L. Berzak Hopkins, S. LePape, L. Divol, A. Pak, E. Dewald, D. D. Ho, N. Meezan, S. Bhandarkar, L. R. Benedetti, and T. Bunn, *Plasma Phys. Controlled Fusion* **61**, 014023 (2019).
- <sup>7</sup>A. L. Kritcher, C. V. Young, H. F. Robey, C. R. Weber, A. B. Zylstra, O. A. Hurricane, D. A. Callahan, J. E. Ralph, J. S. Ross, K. L. Baker *et al.*, “Design of inertial fusion implosions reaching the burning plasma regime,” *Nat. Phys.* **18**, 251–258 (2022).
- <sup>8</sup>A. B. Zylstra, O. A. Hurricane, D. A. Callahan, A. L. Kritcher, J. E. Ralph, H. F. Robey, J. S. Ross, C. V. Young, K. L. Baker, D. T. Casey *et al.*, “Burning plasma achieved in inertial fusion,” *Nature* **601**, 542 (2022).
- <sup>9</sup>H. Abu-Shawareb, R. Acree, P. Adams, J. Adams, B. Addis, R. Aden, 2P. Adrian, B. B. Afeyan, M. Aggleton, L. Aghaian *et al.*, *Phys. Rev. Lett.* **129**, 075001 (2022).
- <sup>10</sup>N. B. Meezan, L. F. Berzak Hopkins, S. Le Pape, L. Divol, A. J. MacKinnon, T. Döppner, D. D. Ho, O. S. Jones, S. F. Khan, T. Ma *et al.*, “Cryogenic tritium-hydrogen deuterium and deuterium-tritium layer implosions with high density carbon ablaters in near-vacuum hohlraums,” *Phys. Plasmas* **22**, 062703 (2015).
- <sup>11</sup>D. S. Clark, C. R. Weber, J. L. Milovich, A. E. Pak, D. T. Casey, B. A. Hammel, D. D. Ho, O. S. Jones, J. M. Koning, A. L. Kritcher *et al.*, “Three-dimensional modeling and hydrodynamic scaling of national ignition facility implosions,” *Phys. Plasmas* **26**, 050601 (2019).
- <sup>12</sup>P. K. Patel, P. T. Springer, C. R. Weber, L. C. Jarrott, O. A. Hurricane, B. Bachmann, K. L. Baker, L. F. Berzak Hopkins, D. A. Callahan, D. T. Casey *et al.*, “Hotspot conditions achieved in inertial confinement fusion experiments on the National Ignition Facility,” *Phys. Plasmas* **27**, 050901 (2020).
- <sup>13</sup>L. Divol, A. Pak, L. F. Berzak Hopkins, S. L. Pape, N. B. Meezan, E. L. Dewald, D. D.-M. Ho, S. F. Khan, A. J. MacKinnon, J. S. Ross *et al.*, “Symmetry control of an indirectly driven high-density-carbon implosion at high convergence and high velocity,” *Phys. Plasmas* **24**, 056309 (2017).
- <sup>14</sup>S. Le Pape, L. Divol, L. Berzak Hopkins, A. MacKinnon, N. B. Meezan, D. Casey, J. Frenje, H. Herrmann, J. McNaney, T. Ma *et al.*, “Observation of a reflected shock in an indirectly driven spherical implosion at the National Ignition Facility,” *Phys. Rev. Lett.* **112**, 225002 (2014).
- <sup>15</sup>R. D. Richtmyer, “Taylor instability in shock acceleration of compressible fluids,” *Commun. Pure Appl. Math.* **13**(2), 297–319 (1960).
- <sup>16</sup>E. E. Meshkov, “Instability of a shock wave accelerated interface between two gases,” *Fluid Dyn.* **4**, 101 (1970).
- <sup>17</sup>G. Dimonte and B. Remington, “Richtmyer-Meshkov experiments on the Nova laser at high compression,” *Phys. Rev. Lett.* **70**, 1806 (1993).
- <sup>18</sup>Lord Rayleigh, “Investigation of the character of the equilibrium of an incompressible heavy fluid of variable density,” *Proc. London Math. Soc.* **s1-s14**, 170 (1882).
- <sup>19</sup>G. Taylor, “The instability of liquid surfaces when accelerated in a direction perpendicular to their planes. I,” *Proc. R. Soc. London, Ser. A* **201**, 192 (1950).
- <sup>20</sup>K. A. Flippo, F. W. Doss, J. L. Kline, E. C. Merritt, D. Capelli, T. Cardenas, B. DeVolder, F. Fierro, C. M. Huntington, L. Kot *et al.*, “Late-time mixing sensitivity to initial broadband surface roughness in high-energy-density shear layers,” *Phys. Rev. Lett.* **117**, 225001 (2016).
- <sup>21</sup>F. W. Doss, J. L. Kline, K. A. Flippo, T. S. Perry, B. G. DeVolder, I. Tregillis, E. N. Loomis, E. C. Merritt, T. J. Murphy, L. Welsch-Sherrill *et al.*, “The shock/shear platform for planar radiation-hydrodynamics experiments on the National Ignition Facility,” *Phys. Plasmas* **22**, 056303 (2015).
- <sup>22</sup>N. Metzler, A. L. Velikovich, and J. H. Gardner, *Phys. Plasmas* **6**, 3283 (1999).
- <sup>23</sup>D. S. Clark, D. T. Casey, C. Weber, O. S. Jones, K. Baker, E. L. Dewald, L. Divol, A. Do, A. L. Kritcher, O. L. Landen *et al.*, “Exploring implosion designs for increased compression on the National Ignition Facility using high density carbon ablaters,” *Phys. Plasmas* **29**, 052710 (2022).
- <sup>24</sup>A. Do, C. R. Weber, E. L. Dewald, D. T. Casey, D. S. Clark, S. F. Khan, O. L. Landen, A. G. MacPhee, and V. A. Smalyuk, *Phys. Rev. Lett.* **129**, 215003 (2022).
- <sup>25</sup>R. Tommasini, D. T. Casey, D. Clark, A. Do, K. L. Baker, O. L. Landen, V. A. Smalyuk, C. Weber, B. Bachmann, E. Hartouni *et al.*, *Phys. Rev. E* (to be published).
- <sup>26</sup>C. R. Weber, D. S. Clark, D. T. Casey, G. N. Hall, O. Jones, O. Landen, A. E. Pak, and V. A. Smalyuk, “Reduced mixing in inertial confinement fusion with early-time interface acceleration,” *Phys. Rev. E* **108**, L023202 (2023).
- <sup>27</sup>H. F. Robey, P. M. Celliers, J. L. Kline, A. J. MacKinnon, T. R. Boehly, O. L. Landen, J. H. Eggert, D. Hicks, S. Le Pape, D. R. Farley *et al.*, *Phys. Rev. Lett.* **108**, 215004 (2012).
- <sup>28</sup>P. M. Celliers and M. Millot, “Imaging velocity interferometer system for any reflector (VISAR) diagnostics for high energy density sciences,” *Rev. Sci. Instrum.* **94**(1), 011101 (2023).
- <sup>29</sup>J. A. Koch, O. L. Landen, B. J. Koziolski, N. Izumi, E. L. Dewald, J. D. Salmonson, and B. A. Hammel, “Refraction-enhanced x-ray radiography for inertial confinement fusion and laser-produced plasma applications,” *J. Appl. Phys.* **105**, 113112 (2009).
- <sup>30</sup>K. Baker, C. Thomas, D. Casey, S. Khan, B. Spears, R. Nora, T. Woods, J. Milovich, R. Berger, D. Strozzi *et al.*, *Phys. Rev. Lett.* **121**, 135001 (2018).
- <sup>31</sup>D. Casey, C. Thomas, K. Baker, B. Spears, M. Hohenberger, S. Khan, R. Nora, C. Weber, D. Woods, and O. Hurricane, *Phys. Plasmas* **25**, 056308 (2018).
- <sup>32</sup>M. M. Marinak, G. D. Kerbel, N. A. Gentile, O. Jones, D. Munro, S. Pollaine, T. R. Dittrich, and S. W. Haan, “Three-dimensional HYDRA simulations of National Ignition Facility targets,” *Phys. Plasmas* **8**(5), 2275 (2001).
- <sup>33</sup>S. Davidovits, C. R. Weber, and D. S. Clark, *Phys. Plasmas* **29**, 112708 (2022).
- <sup>34</sup>J. A. Koch, O. L. Landen, L. J. Suter, L. P. Masse, D. S. Clark, J. S. Ross, A. J. MacKinnon, N. B. Meezan, C. A. Thomas, and Y. Ping, “Refraction-enhanced backlit imaging of axially symmetric inertial confinement fusion plasmas,” *Appl. Opt.* **52**, 3538 (2013).
- <sup>35</sup>E. Dewald, O. Landen, D. Ho, L. Berzak Hopkins, Y. Ping, L. Masse, D. Thorn, J. Kroll, and A. Nikroo, “Direct observation of density gradients in ICF capsule implosions via streaked refraction enhanced radiography (RER),” *High Energy Density Phys.* **36**, 100795 (2020).
- <sup>36</sup>A. Kar, T. R. Boehly, P. B. Radha, D. H. Edgell, S. X. Hu, P. M. Nilson, A. Shvydky, W. Theobald, D. Cao, K. S. Anderson *et al.*, “Simulated refraction-enhanced x-ray radiography of laser-driven shocks,” *Phys. Plasmas* **26**, 032705 (2019).
- <sup>37</sup>E. L. Dewald, R. Tommasini, A. MacKinnon, A. MacPhee, N. Meezan, R. Olson, D. Hicks, S. LePape, N. Izumi, K. Fournier *et al.*, “Capsule ablator inflight performance measurements via streaked radiography of ICF implosions on the NIF,” in 8th International Conference on Inertial Fusion Sciences and Applications, 2016.
- <sup>38</sup>C. Weber, T. Doppner, D. Casey, T. Bunn, L. Carlson, R. Dylla-Spears, B. Koziolski, A. G. MacPhee, J. Sater, A. Nikroo *et al.*, *J. Phys.: Conf. Ser.* **717**, 012057 (2016).
- <sup>39</sup>V. A. Smalyuk, S. X. Hu, J. D. Hager, J. A. Delettrez, D. D. Meyerhofer, T. C. Sangster, and D. Shvarts, *Phys. Rev. Lett.* **103**, 105001 (2009).
- <sup>40</sup>E. L. Dewald, R. Tommasini, N. B. Meezan, O. L. Landen, S. Khan, R. Rygg, J. Field, A. S. Moore, D. Sayre, A. J. MacKinnon *et al.*, *Phys. Plasmas* **25**(9), 092702 (2018).
- <sup>41</sup>J. A. Frenje, R. Bionta, E. J. Bond, J. A. Caggiano, D. T. Casey, C. Cerjan, J. Edwards, M. Eckart, D. N. Fittinghoff, S. Friedrich *et al.*, *Nucl. Fusion* **53**, 043014 (2013).
- <sup>42</sup>V. Y. Glebov, T. C. Sangster, C. Stoeckl, J. P. Knauer, W. Theobald, K. L. Marshall, M. J. Shoup III, T. Buczek, M. Cruz, T. Duffy *et al.*, “The National Ignition Facility neutron time-of-flight system and its initial performance,” *Rev. Sci. Instrum.* **81**, 10D325 (2010).
- <sup>43</sup>O. L. Landen, D. T. Casey, J. M. DiNicola, T. Doeppner, E. P. Hartouni, D. E. Hinkel, L. F. Berzak Hopkins, M. Hohenberger, A. L. Kritcher, S. LePape *et al.*, *High Energy Density Phys.* **36**, 100755 (2020).
- <sup>44</sup>A. J. MacKinnon, N. B. Meezan, J. S. Ross, S. Le Pape, L. Berzak Hopkins, L. Divol, D. Ho, J. Milovich, A. Pak, J. Ralph *et al.*, “High-density carbon ablator experiments on the National Ignition Facility,” *Phys. Plasmas* **21**, 056318 (2014).
- <sup>45</sup>S. Ali, P. Celliers, S. Haan, T. Boehly, N. Whiting, S. Baxamusa, H. Reynolds, M. Johnson, J. Hughes, and B. Watson, *Phys. Plasmas* **25**, 092708 (2018).

- <sup>46</sup>M. J. Edwards, P. K. Patel, J. D. Lindl, L. J. Atherton, S. H. Glenzer, S. W. Haan, J. D. Kilkenny, O. L. Landen, E. I. Moses, A. Nikroo *et al.*, “Progress towards ignition on the National Ignition Facility,” *Phys. Plasmas*. **20**, 070501 (2013).
- <sup>47</sup>D. T. Casey, J. L. Milovich, V. A. Smalyuk, D. S. Clark, H. F. Robey, A. Pak, A. G. MacPhee, K. L. Baker, C. R. Weber, T. Ma *et al.*, “Improved performance of high areal density indirect drive implosions at the National Ignition Facility using a four-shock adiabat shaped drive,” *Phys. Rev. Lett.* **115**, 105001 (2015).
- <sup>48</sup>V. A. Smalyuk, L. J. Atherton, L. R. Benedetti, R. Bionta, D. Bleuel, E. Bond, D. K. Bradley, J. Caggiano, D. A. Callahan, D. T. Casey *et al.*, *Phys. Rev. Lett.* **111**, 215001 (2013).